Human Molecular Genetics, 2016, Vol. 25, No. 9 1824–1835

doi: 10.1093/hmg/ddw054
Advance Access Publication Date: 21 February 2016
Original Article

ORIGINAL ARTICLE

Recessive NEK9 mutation causes a lethal skeletal dysplasia with evidence of cell cycle and ciliary defects

Jillian P. Casey[1,2,*], Kieran Brennan[3], Noemie Scheidel[3], Paul McGettigan[2,4], Paul T. Lavin[3], Stephen Carter[3], Sean Ennis[2], Huw Dorkins[5,6,7], Neeti Ghali[5], Oliver E. Blacque[3], Margaret M. Mc Gee[3], Helen Murphy[8] and Sally Ann Lynch[1,2]

[1]Clinical Genetics, Children's University Hospital, Temple Street, Dublin 1, Ireland, [2]UCD Academic Centre on Rare Diseases, School of Medicine and Medical Sciences, [3]UCD School of Biomolecular & Biomedical Science, Conway Institute, [4]UCD School of Agriculture, Food Science and Veterinary Medicine, University College Dublin, Belfield, Dublin 4, Ireland, [5]North West Thames Regional Genetics Service, Northwick Park Hospital, London North West Healthcare NHS Trust, Watford Road, Harrow HA1 3UJ, UK, [6]Leicestershire Genetics Service, Leicester Royal Infirmary, Leicester LE1 5WW, UK, [7]St Peter's College, University of Oxford, Oxford OX1 2DL, UK and [8]Manchester Academic Health Science Centre, Genetic Medicine-University of Manchester, St Mary's Hospital, Manchester, UK

*To whom correspondence should be addressed at: Clinical Genetics, Children's University Hospital, Temple Street, Dublin 1, Ireland. Tel: +353 1 8784645; Fax: +353 1 8784233; Email: jillian.casey@ucd.ie

Abstract

Skeletal dysplasias are a clinically and genetically heterogeneous group of bone and cartilage disorders. Whilst >450 skeletal dysplasias have been reported, 30% are genetically uncharacterized. We report two Irish Traveller families with a previously undescribed lethal skeletal dysplasia characterized by fetal akinesia, shortening of all long bones, multiple contractures, rib anomalies, thoracic dysplasia, pulmonary hypoplasia and protruding abdomen. Single nucleotide polymorphism homozygosity mapping and whole exome sequencing identified a novel homozygous stop-gain mutation in *NEK9* (c.1489C>T; p.Arg497*) as the cause of this disorder. *NEK9* encodes a never in mitosis gene A-related kinase involved in regulating spindle organization, chromosome alignment, cytokinesis and cell cycle progression. This is the first disorder to be associated with *NEK9* in humans. Analysis of NEK9 protein expression and localization in patient fibroblasts showed complete loss of full-length NEK9 (107 kDa). Functional characterization of patient fibroblasts showed a significant reduction in cell proliferation and a delay in cell cycle progression. We also provide evidence to support possible ciliary associations for NEK9. Firstly, patient fibroblasts displayed a significant reduction in cilia number and length. Secondly, we show that the *NEK9* orthologue in *Caenorhabditis elegans*, *nekl-1*, is almost exclusively expressed in a subset of ciliated cells, a strong indicator of cilia-related functions. In summary, we report the clinical and molecular characterization of a lethal skeletal dysplasia caused by *NEK9* mutation and suggest that this disorder may represent a novel ciliopathy.

Introduction

Skeletal dysplasias are a highly heterogeneous group of disorders affecting bone and cartilage growth. Other organ systems can also be affected. More than 450 different genetic skeletal dysplasias have been documented to date (1). These disorders can vary considerably in their clinical presentation, ranging from mild anomalies and short stature to severe perinatal lethal

Received: December 28, 2015. **Revised and Accepted:** February 15, 2016

disorders with multisystem congenital malformations. Many of the prenatal onset skeletal dysplasias are lethal, often due to dysplasia of the thoracic cavity which results in pulmonary hypoplasia (2). All of the lethal types are associated with short ribs, a small chest circumference and abnormal chest to abdominal circumference ratios for gestational stage (3). This short-rib phenotype can be a useful diagnostic feature detectable by antenatal ultrasound scan from the second trimester onwards (4). It is difficult to accurately determine the prevalence of skeletal dysplasias as the lethal types are likely under-recorded and under-reported. Current estimates are based on studies undertaken up to 20 years ago and range from 0.36 to 3.2 per 10 000 live births (5,6). However, it has been suggested that the real prevalence figures are likely twice that (5), with occurrence during pregnancy being even higher.

Skeletal dysplasias can be caused by autosomal dominant, autosomal recessive or X-linked mutations, in addition to imprinting errors, somatic mosaicism and teratogen exposures (1,7,8). Approximately 70% of the 450 skeletal dysplasias have a known molecular basis (1), with over a hundred yet to be characterized at the molecular level. One complicating factor is the observation that identical phenotypes can be caused by mutations in different genes (9). Conversely, different mutations in the same gene can also give rise to different phenotypes (10), thus complicating clinical diagnosis prior to molecular testing.

The Irish Travellers are an endogamous nomadic group with a tradition of consanguineous marriage. They number ~40 000 in the island of Ireland (Republic of Ireland and Northern Ireland) with a further 5000 in Great Britain. We present two consanguineous Irish Traveller families with a recessive lethal skeletal dysplasia of unknown genetic aetiology (Figs. 1 and 2). The disorder is characterized by fetal akinesia, multiple contractures, shortening of upper and lower limbs, bowed short femurs (in one family), short broad ribs, narrow chest and thorax, pulmonary hypoplasia and protruding abdomen. Detailed clinical information is provided in Table 1. Analysis of cultured fibroblasts showed normal karyotypes in all cases. Whole chromosome aneuploidy and triploidy were excluded by array comparative genomic hybridization and quantitative fluorescence polymerase chain reaction (PCR), respectively. Diagnostic sequencing of *CHRND*, *DOK7* and *RAPSN* was normal. Metabolic testing on fibroblasts from post-termination skin biopsy included normal free carnitine/acyl carnitine and a normal lysosomal enzyme screen. We aimed to identify the underlying disease gene for this lethal skeletal dysplasia using the combined approach of single nucleotide polymorphism (SNP) homozygosity mapping and whole exome sequencing.

Results

Homozygosity mapping and exome sequencing in family A

SNP homozygosity mapping of DNA from baby A:IV:1 identified nine regions of homozygosity (ROH) >3 Mb containing 941 positional candidate genes (Supplementary Material, Fig. S1). None of these genes had previously been associated with a lethal skeletal dysplasia. Therefore, exome sequencing was undertaken for the proband (A:IV:1) and one unaffected sibling. Assuming an autosomal recessive model, we prioritized autosomal variants that were (i) homozygous, (ii) absent or present with a frequency of <1% in dbSNP142, NHLBI Exome Variant Server database and 1000 Genomes, (iii) coding (missense, nonsense, splice site and indels), (iv) located within the nine candidate homozygous regions, (v) homozygous normal or heterozygous in the unaffected sibling and (vi) absent in our 70 Irish control exomes (Supplementary Material, Table S2). This prioritization strategy identified two novel candidate variants: a missense variant in *WDR52* (NM_001164496.1 c.2006T>C p.(Met669Thr)) and a stop-gain variant in *NEK9* [MIM *609798] (NM_033116.4 c.1489C>T p.Arg497*).

Both variants were validated by Sanger sequencing. However, the variant in *WDR52* did not segregate with the phenotype and was excluded (not shown). In contrast, the stop-gain variant in *NEK9* fully segregated with the disorder (Fig. 1D). *NEK9* is one of 11 members of the never in mitosis gene A (NIMA) family of protein kinases. The NEK genes are involved in different biological functions including cell cycle control, the DNA damage response, primary cilium formation and apoptosis signalling (11–13). Specifically, *NEK9* is involved in regulating spindle organization, chromosome alignment, cytokinesis and normal cell cycle progression (14–17). Mutations in *NEK9* have not previously been associated with any disorder in humans. However, a mutant *Nek9* mouse created by the Wellcome Trust Sanger Institute showed pre-weaning lethality (Mouse Genome Database).

The identified stop-gain variant results in protein truncation at residue 497. As a result, the mutant NEK9 protein is predicted to be missing 49% (483/980) of its amino acids compared with the wild-type protein (Supplementary Material, Fig. S2). The wild-type NEK9 protein comprises an N-terminal protein kinase domain (52-308), a nuclear localization signal (306-330), a central RCC1-like domain (388-726), a NEK6 interaction region (732-891) and a C-terminal coiled-coil domain (892-939) (15). Critically, the truncated mutant protein lacks the majority of the RCC1-like domain, with complete loss of the NEK6 interaction region and the coiled-coil domain.

Identification of a second family

Subsequently, an additional Irish Traveller family was identified with a similar clinical history (Table 1 and Fig. 2). Family B includes three fetuses with an undiagnosed lethal skeletal dysplasia. Whilst the exact relationship between Families A and B is unknown, it is believed that they are distantly related. SNP homozygosity mapping of patient B:III:4 identified 11 ROH >3 Mb (Supplementary Material, Fig. S3). Comparison of the ROH in Families A and B identified only one homozygous region shared by both families on chromosome 14q24.1–q24.3 (chr14:69830974–76961560). The overlapping region measures 7.13 Mb and contains 74 genes, including *NEK9* (Supplementary Material, Fig. S4). As each disorder within the Irish Traveller population tends to be caused by a common homozygous mutation due to founder effects, we proceeded to test Family B for the *NEK9* c.1489C>T stop-gain variant identified by whole exome sequencing in Family A. Sanger sequencing in Family B showed that the two fetuses are homozygous for the *NEK9* stop-gain variant, the unaffected parents are obligate carriers and the unaffected siblings are not homozygous for this variant. DNA was not available from the third fetus B:III:3. Considering both families together, the *NEK9* c.1489C>T variant shows complete segregation amongst four affected fetuses, four carrier parents and five unaffected siblings.

Analysis of NEK9 protein levels in patient fibroblasts

Analysis of NEK9 protein expression in patient fibroblasts showed that the R497* mutation resulted in complete loss of the full-length wild-type NEK9 protein. The predicted 55 kDa truncated mutant protein was not detected in the patient fibroblasts using two different antibodies (Fig. 3A and Supplementary Material, Fig. S5), which may be due to nonsense-mediated

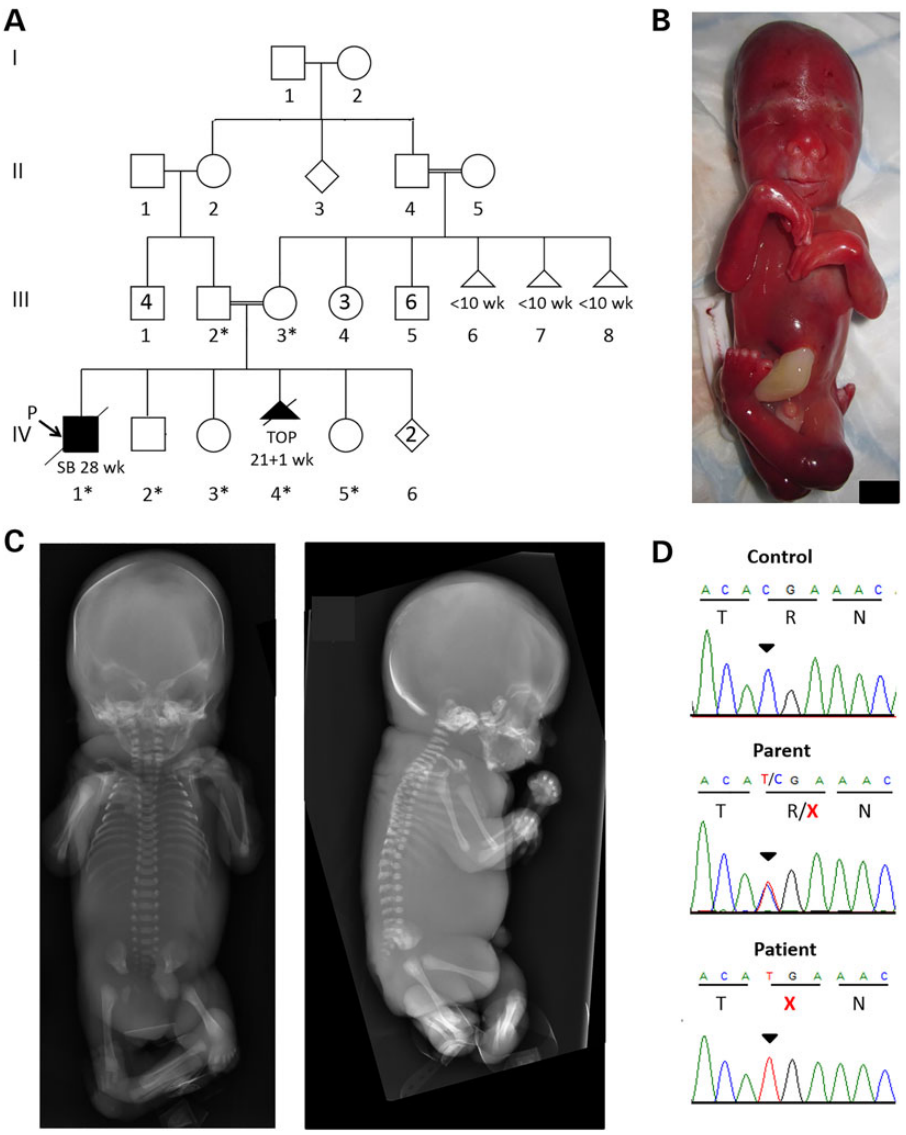

Figure 1. Family A. (**A**) Pedigree of consanguineous Irish Traveller family who had two babies affected with a lethal skeletal dysplasia. DNA samples were available from individuals denoted with an asterisk. Pedigree symbols are as follows: squares, males; circles, females; diamonds, sex not specified; filled symbols, affected individual with lethal skeletal dysplasia; diagonal line through symbols, individual is deceased; triangles, miscarried embryos (<10 weeks); filled triangle with diagonal line, affected TOP (sex not specified). Abbreviations: P, proband; SB, still birth; TOP, termination of pregnancy. (**B**) Photograph of baby A:IV:4 showing a long narrow head, long philtrum and fixed flexion deformities of the wrists, elbows, hips and knees. (**C**) Anteroposterior (AP) and lateral post-mortem X-rays of baby A:IV:1 showing fixed flexion deformities of upper and lower limbs, with a delayed bone age (poor ossification of the os calcis). Ribs are abnormally modelled with a ribbon appearance and sclerotic areas in left fourth to sixth ribs. A reversed thoracic kyphosis and pronounced soft tissue thickening are also observed. (**D**) Sanger sequence validation of the *NEK9* c.1489C>T variant identified by whole exome sequencing. Representative Sanger traces from a population control (homozygous normal), carrier parent (heterozygous) and affected baby (homozygous for mutation). The C>T transition is denoted by an inverted black triangle and results in a premature stop codon at amino acid 497.

degradation of mRNA from the mutant allele as a result of the premature termination mutation.

Analysis of cell cycle progression in patient fibroblasts

NEK9 has been shown to modulate interphase progression via its association with the FACT (Facilitates Chromatin Transcription) complex. FACT comprises two highly conserved subunits encoded by SUPT16H (also called Spt16) and SSRP1 (18). This multiprotein complex functions as a chromatin-specific transcription elongation factor with important roles in replication and transcription. Autophosphorylated NEK9 associates with FACT during G1/S transition and S-phase progression, with loss of NEK9 prolonging G1 and S phases (19). Given the implication of NEK9 in the regulation of cell cycle progression, we examined the rate of cell proliferation and cell cycle progression in the patient fibroblasts compared with control cells that contained full-length NEK9. MTT assay results show a significant reduction in the proliferation of patient cells compared with normal counterparts ($^{***}P < 0.001$) (Fig. 3B). Cells were then synchronized at the G1/S boundary by double thymidine block and subsequently released into S-phase. Cell cycle progression was analysed by DNA content following propidium iodide staining. The percentage of control fibroblasts in S-phase had returned to the constant level of ~30% within

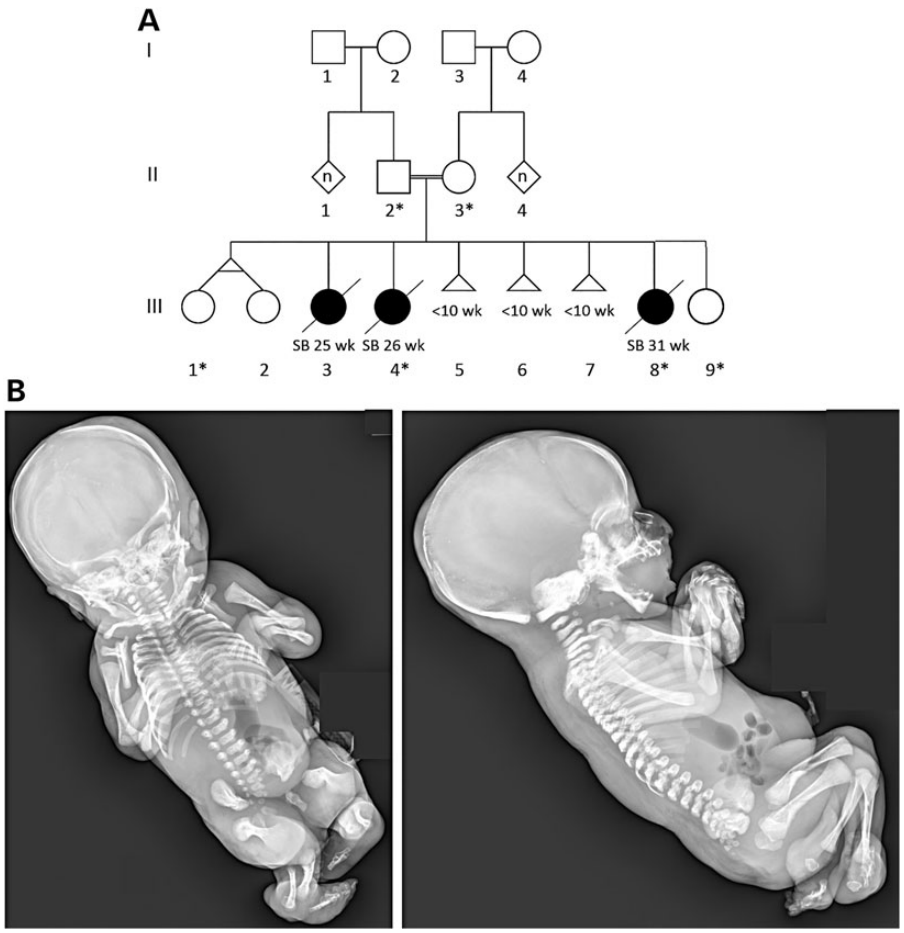

Figure 2. Family B. (**A**) Pedigree of consanguineous Irish Traveller family who had three babies with a lethal skeletal dysplasia. All three babies were stillborn (SB). DNA was available from individuals denoted with an asterisk. Pedigree symbols are as follows: squares, males; circles, females; diamonds, gender not specified; filled symbol, affected individual with lethal skeletal dysplasia; diagonal line through symbols, individual is deceased; triangles, miscarried embryos (<10 weeks); n, multiple individuals but exact number not known. (**B**) Whole body post-mortem X-ray of baby B:III:8 shows broad ribs and wide metaphyses. The vertebrae appear hypoplastic with narrowing of the AP diameter at the upper end plates of the lumbar vertebrae and medial broadening of the clavicles. The vertebrae are short and narrowed, especially at the thoracic level.

10 h, whilst the percentage of patient fibroblasts in S-phase continued to drop to a constant level of ~8% by 12 h (Fig. 3C). This reduction in the level of cells re-entering S-phase is likely due to delayed cell cycle progression and is supported by the finding of reduced proliferation of patient fibroblasts (Fig. 3B). The additional 2 h required by the patient fibroblasts to leave the G1/S boundary and progress through S-phase into G2/M suggests that the R497* mutation may prevent the timely progression of cells through the G1/S boundary and S-phase.

Analysis of cilia in patient fibroblasts

Given the involvement of some NEK genes in ciliary function, and the association of short-rib dysplasia with disruption of known ciliary genes (20–22), we investigated the cilia in the NEK9 R497* patient fibroblasts. The patient fibroblasts displayed a significant reduction in cilia number and length compared with control fibroblasts (***$P < 0.001$) (Fig. 3D–F). The decrease in cilia number and length in NEK9 mutant fibroblasts together with the ciliopathy-related clinical features seen in the patients (including shortened bones, rib anomalies, thoracic dysplasia, flexion contractures, metaphyseal abnormalities, early embryonic death) suggests that the NEK9 R497* mutation may impair ciliary function.

Analysis of *Nekl-1* expression in *C. elegans*

To provide further evidence of possible ciliary associations for *NEK9*, we turned to the roundworm *C. elegans*, which is a robust model for investigating the functions of conserved cilia-related genes (23–25). First we used BLAST to identify *C. elegans* NEKL-1 as the top NEK9 hit ($1e^{-96}$) by sequence homology, followed by a more distantly related NEKL-3 ($1e^{-36}$) protein. The CeNEKL-1 and HsNEK9 proteins are both ~980 amino acids long, displaying 68% similarity (25% identical) at aligned positions. Both proteins possess N-terminal kinase domains, followed by 4-6 RCC1 domains, and a C-terminal coiled-coil dimerization domain (Fig. 4A). Thus, NEKL-1 is the likely orthologue of NEK9. However, NEKL-1 also shares a similar level of sequence similarity with NEK8, indicating that NEKL-1 may be orthologous to both NEK8 and NEK9, although NEK8 is a shorter protein (692 aa) and lacks the C-terminal dimerization motif present in human NEK9 and *C. elegans* NEKL-1.

We examined the tissue expression pattern of *nekl-1* using a reporter comprised of green fluorescent protein (GFP) under the control of *nekl-1* 5′ UTR (promoter) sequence (Fig. 4B). In hermaphrodite worms, only 60 out of 959 cells are ciliated; all of these are sensory neurons, with most located in the head and tail of the animal. In transgenic worms expressing *nekl-1p::gfp*,

Table 1. Summary of the clinical, radiological and histopathological findings

	AIV:1 (male)	A:IV:4 (male)	B:III:3 (female)	B:III:4 (female)	B:III:8 (female)
Antenatal details					
GA at antenatal scan (weeks)	24	20	24	20	28 and 30
Antenatal findings	Fetal akinesia in the context of a severe skeletal dysplasia	Small thorax and restricted movement of the limbs	Early onset IUGR, oligohydramnios, double outlet ventricles, over-riding aorta, crumpled limbs, bilateral talipes	Early hydrops fetalis, decreased movement, bilateral talipes, kinked spine, legs fixed in flexion, omphalocoele	IUGR, radial ray malformation of both hands, femur length less than expected, bowing of femur
Short long bones	+ (<3rd centile)	+	NS	+ (<3rd centile)	+
Birth					
Birth	SVD 28 + 4 weeks GA resuscitation failed	TOP at 21 + 1 weeks GA	SVD 26 weeks GA Baby lived for 1 h	SVD 26 + 4 weeks GA IUFD—not resuscitated	SVD 31 weeks GA resuscitation failed
Weight	892 g (2nd–9th centiles)	260.85 g	NA	630 g	890 g
OFC	25 cm (9th centile)	17.5 cm	NA	23.3 cm (<3rd centile)	25.5 cm (<3rd centile)
Small for GA	+	+ (18–19 weeks GA)	NA	+ (18–25 weeks GA)	+ (25–26 weeks GA)
Post-mortem findings					
Shortening of all four limbs	+	+		+	+
Contractures of all major joints[a]	+	+		+	+
Facial dysmorphism	Micrognathia	Long narrow head, long philtrum, high arched palate (no cleft), micrognathia		Small eyes, low-set ears, long philtrum, small chin, narrow palate	Beaked nose with a saddle bridge, long philtrum, macroglossia, sunken and downward-slanting eyes
Neck	Short with reduced flexion	Short and stiff		Short with right torticollis	NS
Thorax	Small and barrel shaped, reversed thoracic kyphosis	NS		Thoracic scoliosis, narrow pear-shaped small chest, diaphragm intact but bulging upwards, epiglottis mis-shaped, trachea and larynx narrowed	NS
Bilateral talipes	+	+		+	+
Digits	Long overlapping fingers, adducted thumbs	Overlapping fingers, adducted thumbs		Lateral deviation of fingers, abnormal palmar creases	NS
Lung hypoplasia	NS	+		+	+
Other organs	NS	Enlarged heart, liver and kidneys; small thymus and spleen		Small thymus, spleen and adrenals	No renal cysts or hydronephrosis
Brain	NE	Normal, no focal lesions		NE	Normal, CV vermis intact, CC normal, CH of normal size, normal gyral pattern

Table continues

Table 1. Continued

	AIV:1 (male)	A:IV:4 (male)	B:III:3 (female)	B:III:4 (female)	B:III:8 (female)
Other	Narrow hips with right-sided hydrocele	Hips and shoulders internally rotated, appearance of pterygia secondary to severe contractures		Protuberant abdomen, inwardly and upwardly deviated feet, oedema, bulging forehead	Large omphalocoele
X-ray findings					
Shortened long bones	+	+		+	+
Bowing	–	–		+ (short femurs)	+ (bowed femurs)
Ribs	Normal length, modelling deformity, ribbon appearance, localized thickening and sclerosis of the lateral aspect of the left fourth and fifth ribs	X-ray images not available		Broad short ribs, narrow rib cage	Broad ribs with wide metaphyses
Broad metaphyses	–	–		+	+
Other	Delayed bone age, bilateral cervical ribs	Abnormal widening of the distance between C1 and C2		Narrowed short vertebrae, VSD	Hypoplastic vertebrae, medial broadening of the clavicles, VSD
Muscle biopsy					
Findings	Normal histology and fibre size	variation in fibre size with some very small fibres		Changes most compatible with central denervation	NP

Summary of the clinical, radiological and histopathological findings in two Irish Traveller families with a recessive lethal skeletal dysplasia due to *NEK9* mutation. Post-mortem was not performed for baby B:III:3. Eyelids, hair pattern, ears, palate, nails, skin and genitalia were normal in all babies.

Abbreviations: CC, corpus callosum; CV, cerebellar vermis; CH, cerebellar hemispheres; IUFD, intrauterine fetal death; IUGR, intrauterine growth restriction; NA, not available; NE, not examined; NS, not specified; NP, not performed; SVD, spontaneous vaginal delivery; TOP, termination of pregnancy; VSD, ventricular septal defect.

[a]Major joints refers to the elbows, wrists, hips, knees and ankles.

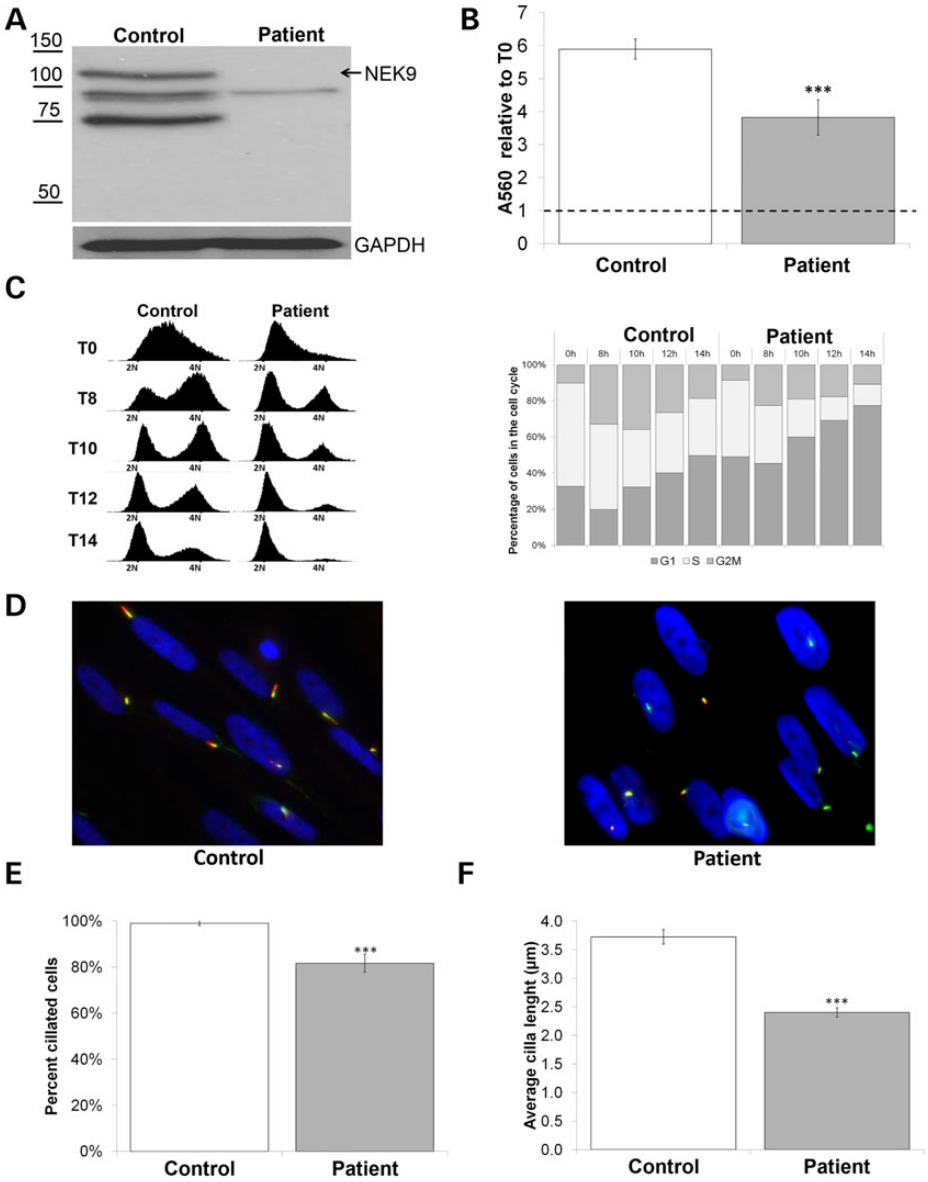

Figure 3. Patient fibroblasts with the NEK9 R497* mutation have reduced cell proliferation with prolonged S-phase and a reduced number of ciliated cells with shorter cilia. (**A**) Full-length and truncated NEK9 protein expression in control and patient (A:IV:4) fibroblasts. Cell extracts were separated by SDS–PAGE and immunoblotted with anti-human NEK9 (Abcam, Cambridge, UK) or GAPDH (Merck Millipore, Darmstadt, Germany). A representative western blot from control and patient fibroblasts is shown. (**B**) The rate of cell proliferation in control and patient fibroblasts was assessed by MTT assay on Day 0 (24 h post seeding) and Day 3, with the fold change in absorbance on Day 3 expressed relative to Day 0. Error bars refer to standard error of the mean of three experiments. (**C**) Control and patient fibroblasts were synchronized at the G1/S junction by a double thymidine block and released into fresh medium. At the indicated time points after release, cells were harvested and subjected to DNA content analysis by FACS, with the percentage change of cells in S-phase at the indicated time points expressed relative to T0. (**D**) Indirect immunofluorescence analysis was performed on control (left panel) and patient (right panel) cells after 72 h serum starvation to observe cilia using anti-human ARL13B (Proteintech, Chicago, IL, USA) (Red), acetylated tubulin (mouse hybridoma C3B9) (Green) and nuclear DNA was counter-stained by DAPI (Blue). Graphic representation of differences in (**E**) the percentage of ciliated cells and (**F**) the average cilia length in patient and control fibroblasts from 12 independent fields of view (***$P < 0.001$).

co-stained with a dye (DiI) that labels a subset of amphid and phasmid ciliated cells (27), we found that the reporter was expressed almost exclusively in a subset of ciliated cells, with little or no obvious expression in non-ciliated cells (Fig. 4B). These cells included all of the ciliated cells in the nematode tail (PHA/B, PQR) and a subset of amphid channel cells in the nematode head (Fig. 4B). Thus, like orthologues of known ciliopathy genes associated with skeletal malformations such as short-rib polydactyly (23,24), the NEK9 orthologue NEKL-1 is expressed only in cells with a primary cilium, which is a strong indicator of a cilia-related function.

Discussion

Our findings show that recessive mutations in *NEK9* cause a lethal skeletal dysplasia characterized by fetal akinesia, multiple contractures, shortened long bones, thoracic dysplasia, pulmonary hypoplasia and protruding abdomen. It is important to note that the main features apparent on antenatal ultrasound are the small rib cage, contractures, pulmonary hypoplasia and protruding abdomen. The skeletal features associated with this *NEK9* disorder are variable and non-specific and are only identifiable on post-mortem full body X-ray.

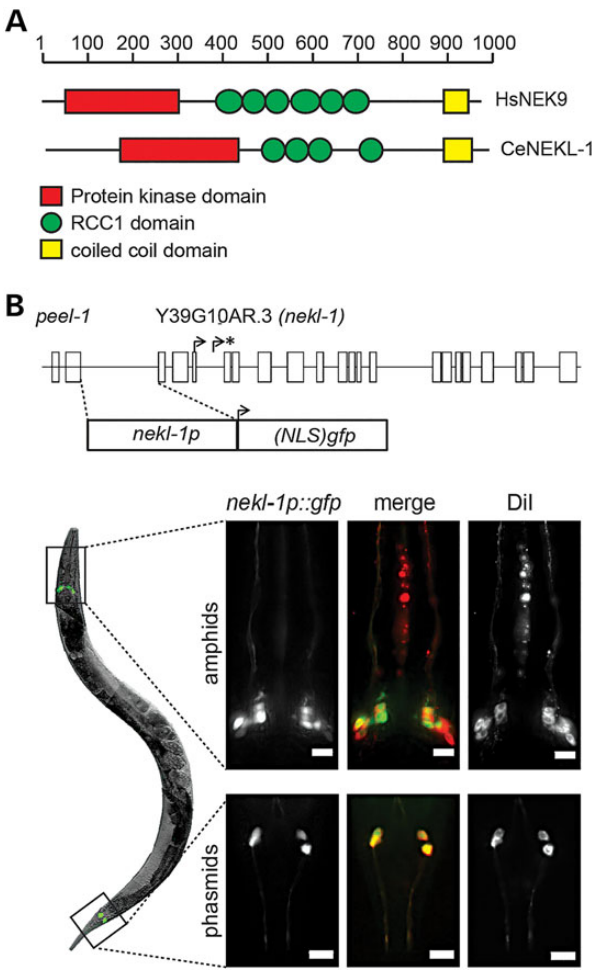

Figure 4. (**A**) *Caenorhabditis elegans* NEK9 orthologue, NEKL-1, is expressed exclusively in ciliated cells. (**a**) Schematic showing the domain organization of human (Hs) NEK9 (NP_149107.4) and *C. elegans* (Ce) NEKL-1 (NP_001293320.1) proteins. Protein kinase and RCC1 domains identified using PROSITE (http://prosite.expasy.org/) and coiled-coil domains identified using COILS (26). RCC1; Regulator of Chromosome Condensation 1. Ruler above schematic denotes amino acid number. (**B**) A GFP reporter under the control of the *nekl-1* promoter sequence is expressed exclusively in ciliated cells. Schematic shows the genomic organization of the *nekl-1* gene and the 5′UTR intergenic sequence used in the GFP reporter (*nekl-1p::gfp*). Exons denoted by boxes. Arrow, start codon of isoform A; arrow star, start codon of isoform B; NLS, nuclear localization sequence. Images taken from transgenic worms expressing *nekl-1p::gfp*. Left image of an entire worm shows GFP expression in a limited number of head and tail cells. Right images show the head and tail regions at higher magnifications and reveal that GFP is expressed in amphid and phasmid ciliated cells that incorporate the fluorescent dye, DiI. Scale bars: 10 μm.

The novel stop-gain mutation (R497*) results in complete loss of the wild-type full-length NEK9 protein. The predicted 55 kDa truncated mutant protein was not detected by western blot in the patient fibroblasts using two different antibodies suggesting that the mutant mRNA is degraded. A number of cell cycle defects were observed in the patient fibroblasts including a reduced proliferation capability and delayed cell cycle progression through the G1/S boundary and S-phase. These findings are consistent with reports that NEK9 is important for interphase progression (19). Alterations in cell cycle regulation have been implicated in the pathogenesis of other embryonic lethal syndromes similar to the NEK9 phenotype including hydrolethalus syndrome (*HYLS1* mutation) and short-rib thoracic dysplasia 6 (*NEK1* mutation) (28,29). The proper level of cell proliferation is critical to normal organ development (30). We speculate that the defects in cell proliferation and cell cycle progression may contribute to the abnormalities in organ size observed in the babies reported here. They may also account, at least in part, for the associated growth abnormalities as all five affected babies were small for gestational age. Furthermore, all babies had hypoplastic lungs, a feature previously linked to alterations in the cell cycle (31,32). Van Loenhout *et al.* specifically showed that a decrease in cells in the S-phase contributes to the pathogenesis of lung hypoplasia (33). We identified a significant delay in G1 to S-phase transition in our patient fibroblasts and propose that this defect contributes to the lung hypoplasia observed in this NEK9-associated skeletal dysplasia.

Humans encode 11 distinct NEK (NIMA-related kinases) genes, named *NEK1* to *NEK11*. The NEK genes encode serine/threonine kinases with diverse biological roles, including cell cycle control, cilia regulation and DNA damage sensing and repair (11,34,35). A number of NEK genes have been associated with recessive disorders in humans, including lethal phenotypes. *NEK1* mutations cause a lethal short-rib polydactyly syndrome Majewski type (MIM 263520), defined by horizontally located short ribs, a hypoplastic thorax, polysyndactyly, micromelia and characteristic disproportionate shortening of the tibiae (22). A recessive truncating mutation in *NEK2* has been identified in a patient with retinitis pigmentosa (MIM 615565) (36). *NEK2* has also been implicated in left–right asymmetry in humans and Xenopus (37). Missense (likely hypomorphic) *NEK8* mutations have been reported in a small number of patients with nephronophthisis type 9 (MIM 613824), suggesting that *NEK8* may be a rare cause of the disorder (38). A loss-of-function nonsense *NEK8* mutation was identified in three fetuses with severe renal–hepatic–pancreatic dysplasia 2 (MIM 615415) (39). This multisystem ciliopathy is characterized by enlarged organs, cystic-dysplastic kidneys and liver, congenital heart defects and bowed femur with shortening of the legs. Pathogenic mutations in *NEK7* have not been reported in humans. However, the absence of Nek7 in mice is lethal in late embryogenesis or during the early postnatal stages and results in severe growth retardation (40).

The clinical features of patients with *NEK1* and *NEK9* mutations show considerable overlap. Both cohorts of patients present with shortening of the ribs, shortening of the bones of all four extremities, a narrow thorax and hypoplastic lungs and epiglottis, with additional variable features including a ventriculoseptal defect, bulging forehead, protruding abdomen and genital anomalies. However, patients with *NEK1* and *NEK9* mutations also have unique features which are not shared between the two syndromes. For example, patients with *NEK1* mutations have a cleft lip and palate, polysyndactyly, renal cysts and extreme shortening of the tibia. These features are not observed (to date) in patients with the *NEK9* skeletal dysplasia. In contrast, patients with *NEK9* mutations present with multiple contractures and short bowed femurs which are not observed in the *NEK1* disorder. Whilst only Family B in the current study had bowed femurs, we cannot exclude the possibility of bowing in Family A as only one X-ray was available and the quality was suboptimal. The presence or absence of these specific features may help with differential diagnosis and to guide appropriate molecular testing.

Thiel *et al.* showed that the *NEK1*-associated osteochondrodysplasia results from a defect in ciliogenesis, with patient fibroblasts showing a significant reduction in cilia number together with structural abnormalities of remaining cilia (22). Similarly, disease-causing mutations in *NEK8* affected ciliary and centrosomal localization (38). Mouse models affecting either Nek1 or Nek8

protein function show phenotypic overlap with ciliopathies (41,42). Notably, all of the known disease genes associated with short-rib polydactyly syndromes to date involve the cilia cycle. This observation, together with the phenotypic overlap with *NEK1* patients, prompted our hypothesis that the *NEK9*-associated skeletal dysplasia could be caused by ciliary dysfunction. Indeed, analysis of *NEK9* patient fibroblasts showed a significant reduction in cilia number and length, similar to the findings in *NEK1* patients. Analysis of the human NEK9 orthologue in *C. elegans* (NEKL-1) showed that *nekl-1* has a restrictive expression pattern and is exclusively limited to a subset of ciliated cells. Other ciliopathy genes, such as those genes involved in the Bardet–Biedl syndrome and the skeletal-associated Jeune syndrome, show the same type of restricted expression pattern, which is typically a strong indicator of a genes' involvement in ciliary function.

The potential involvement of human NEK9 in ciliary function is not altogether surprising given its similarity to NEK8, a gene known to be involved in ciliogenesis (38,43). Phylogenetic analysis suggests that human NEK8 and NEK9 form a subfamily within the Nek family (34,44,45). Both genes have a kinase domain and regulator of chromosome condensation (RCC1) and autophosphorylate in the non-catalytic C-terminal region to regulate their localization and/or activation (43,46). In addition, mutation of NEK8 causes skeletal anomalies similar to NEK9 (shortened long bones and bowed femur), although the phenotype in NEK8 ciliopathies is clearly broader (39). The Nek8–Nek9 subfamily is also observed in plants (47). In plants, there is evidence that large-scale whole genome duplication events followed by extensive reshuffling and divergent evolution likely shaped the NEK gene family (47). Could this also hold true for humans? It is plausible that the present NEK8 and NEK9 in humans could be represented by a single ancestral gene in lower eukaryotes. This ancestral gene may have undergone duplication, with subsequent truncation to give rise to human NEK8 which is much shorter and lacks some of the domains present in NEK9. The *C. elegans* BLAST results presented in this study support this hypothesis. *C. elegans* NEKL-1 is the top hit for human NEK9, but NEKL-1 also shows high homology to human NEK8. Of the two genes, NEKL-1 shows greater similarity to human NEK9. Both are of similar length and possess the same protein domains organized in the same manner; an N-terminal kinase domain followed by 4–6 RCC1 domains, and a C-terminal coiled-coil dimerization domain. In contrast, NEK8 is much shorter than NEKL-1 and lacks the C-terminal dimerization motif. Therefore, whilst NEKL-1 may represent the true orthologue of NEK9, our findings raise interesting questions regarding the ancestral origin of the NEK8–NEK9 subfamily.

The presence of contractures in all five babies with the *NEK9*-associated skeletal dysplasia is noteworthy. Contractures are not a common feature of ciliopathies but have been reported in some patients with ciliary dysfunction. Firstly, oral–facial–digital syndrome is caused by mutations in the *OFD1* gene which plays a critical role in primary cilia function. Occasionally, this syndrome includes generalized contractures or contractures of the knees (48,49). Secondly, the Marden–Walker syndrome includes multiple joint contractures and is linked to dysfunctional mechanisms in the primary cilia structures of the cell (50). One gene associated with the Marden–Walker syndrome, *PIEZO2*, has also been shown to cause a subtype of distal arthrogryposis (51). A role for cilia in chondrocyte development has been established (52), and correct cilia function is critical to neural patterning, progenitor proliferation, cell migration and axon guidance in the developing human brain and spinal cord (53). Ciliary defects are likely to adversely affect multiple developmental pathways (54). It is plausible that the contractures may not be a direct result of NEK9 deficiency itself but rather the elimination of an interaction between NEK9 and a critical binding partner(s) involved in bone development. Future investigations into the exact role of NEK9 in ciliary function and bone development may help to determine how NEK9 deficiency leads to severe contractures.

In summary, we have identified *NEK9* as the cause of a lethal recessive skeletal dysplasia, which is the first disorder to be associated with *NEK9* in humans to date. We anticipate that many more cases of this *NEK9*-associated disorder are yet to be identified and will help to define the phenotypic spectrum of this skeletal dysplasia. We provide evidence of cell cycle and ciliary defects in patient fibroblasts, providing insight into the molecular mechanism of this skeletal dysplasia. Finding that expression of the NEK9 orthologue in *C. elegans* is restricted to ciliated cells adds further support for a potential role of *NEK9* in ciliary function. Taken together, our findings suggest that *NEK9* could represent a ciliopathy and future investigations into the potential role of *NEK9* in ciliary function are warranted.

Materials and Methods

Ethics and consent

The study was approved by the Ethics Committee of Temple Street Children's University Hospital (Dublin, Ireland). Written informed consent was obtained from the parents, including consent to publish patient photographs.

SNP genotyping

In Family A, DNA samples were available from two affected babies (A:IV:1 and A:IV:4), three unaffected siblings (A:IV:2, A:IV:3 and A:IV:5) and both parents (A:III:2 and A:III:3). In Family B, DNA was available from two affected babies (B:III:4 and B:III:8), two unaffected siblings (B:III:1 and B:III:9) and both parents (B:II:2 and B:II:3). Genomic DNA was extracted from peripheral lymphocytes. DNA from patients A:IV:1 and B:III:4 was genotyped for 964 193 SNPs on an Illumina BeadStation 500GX platform using the Illumina Omni Human OmniExpressExome array (AROS Applied Biotechnology, Aarhus N, Denmark). ROH >3 Mb were identified using plink and compared to identify ROH common to both families (55).

Whole exome sequencing

DNA from one affected fetus (A:IV:4) and one healthy sibling was selected for exome sequencing. Whole exome targeted capture was performed using the SureSelect v5 50 Mb Human All Exon Kit (Agilent Technologies, Santa Clara, CA, USA). Sequencing was performed on an Illumina HiSeq (Illumina) at GATC Biotech (Konstanz, Germany). The reads were aligned to the hg19 reference genome using BWA version 0.5.7 (56). Duplicates were removed, and the quality scores for the aligned reads were recalibrated using genome analysis toolkit (57). Variants and indels were identified using SAMtools and annotated with ANNOVAR (58,59).

Validation and segregation analysis

Validation and segregation analysis of the *NEK9* NM_033116.4 c.1489C>T and *WDR52* NM_001164496.1 c.2006T>C variants was undertaken by PCR and Sanger sequencing (Supplementary Material, Table S1). The identified *NEK9* variant was submitted to http://databases.lovd.nl/shared/genes/NEK9.

Cell culture

The MRC5 fetal fibroblast cell line was obtained from American Type Culture Collection and was used as a control. Patient fibroblasts were available from one baby in Family A and were obtained according to routine hospital protocols. Cells were grown under standard conditions at 37°C at 5% CO_2 (DMEM, 20% fetal bovine serum, 50 IU/ml penicillin, 50 µg/ml streptomycin).

Antibodies

Anti-human antibodies for western blotting and immunofluorescence analyses were sourced as follows: rabbit ARL13B (Proteintech, Chicago, IL, USA), rabbit NEK9 (Ab138488, Abcam, Cambridge, UK), mouse NEK9 (Ab57925, Abcam, Cambridge, UK), mouse GADPH (Merck Millipore, Darmstadt, Germany) and mouse acetylated tubulin (Sigma-Aldrich Cat. No. T7451, clone 6-44 11B-1). Horseradish peroxidase-conjugated anti-rabbit and anti-mouse secondary antibodies (Cell Signaling Technology) and AlexaFluor488, AlexaFluor596-conjugated anti-rabbit and anti-mouse secondary antibodies (Thermo Fisher Scientific, Waltham, MA, USA).

Western blotting

Patient and control fibroblasts were harvested at 80% confluency, washed in PBS, and lysed in RIPA lysis buffer [Tris/Cl (10 mM pH 7.5), NaCl (150 mM), NP-40 (1%), sodium deoxycholate (0.25%), PMSF (100 µM), NaF (1 mM), aprotinin (10 µg/ml), leupeptin (10 µg/ml), pepstatin (10 µg/ml), Na_3VO_4 (100 µM) and β-glycerophosphate (100 µM)]. Protein concentration was determined by the Bradford reagent (Bio-Rad). Protein samples were separated by SDS–PAGE under reducing conditions by using Tris-glycine running buffer. After electrophoresis, proteins were transferred to PVDF membranes (Immobilon; Millipore). Membranes were blocked in 5% BSA for 1 h and incubated overnight with primary antibody at 4°C. Membranes were washed and incubated for 1 h with HRP-conjugated secondary antibodies. Protein was detected using Western Lightning Enhanced Chemiluminescence reagent (Thermo Fisher Scientific, Waltham, MA, USA).

Immunofluorescence

Patient and control fibroblasts were grown on coverslips and fixed in 1% paraformaldehyde for 30 min then washed in PBS, and slides were allowed to air-dry. Cells were then incubated in 0.5% (v/v) Triton-X-100 in PBS for 30 min, and the cells were again washed in PBS and slides allowed to air-dry. The cells were blocked in 5% BSA in PBS for 30 min, then washed once in PBS and incubated with primary antibody (1:100 dilution) overnight at 4°C in a humidity chamber. The cells were again washed in PBS and incubated in secondary fluorescent antibody (1:1000 dilution) for 1 h at room temperature in the dark. The cells were washed in PBS and stained with 4′,6-diamidino-2-phenylindole (DAPI) (1 µg/ml) for 20 s and washed for a final time in PBS. Coverslips were mounted using a drop of fluorescent mounting medium (Dako). The stained cells were visualized using the AxioImager 2 epifluorescent microscope (Zeiss), and images were captured using the AxioVision software.

Measurement of cell proliferation

The MTT colorimetric assay was used to measure the rate of cell proliferation in patient and control fibroblasts on Day 0 (24 h post seeding) and Day 3. Fibroblasts were grown in a 96-well plate at 2000 cells per well in 200 µl of medium. MTT, a tetrazolium dye (3-[4, 5-dimethylthiazol-2-yl]-2, 5-diphenyltetrazolium bromide; thiazolyl blue, Sigma, St. Louis, MO, USA) was added to each well in the assay in a volume of 20 µl at a concentration of 5 mg/ml MTT. The plates were incubated in the presence of MTT dye for 5 h. Mitochondrial dehydrogenase activity reduced the yellow MTT dye to a purple formazan, which was then solubilized with DMSO and absorbance was read at 560 nm on an ELISA plate reader.

Cell cycle synchronization and propidium iodide staining

Cells were synchronized at the G1/S boundary by double thymidine block. Subconfluent culture was blocked with 2 mM thymidine and incubated for 16 h. The cells were washed three times with PBS and then incubated with fresh serum-rich medium for 12 h. The cells were cultured again with media containing 2 mM thymidine for an additional 24 h. The cells were released from the G1/S block by three washes with PBS and collected by trypsinization at the indicated time points. The cells were fixed with 70% ethanol at 4°C overnight. Following overnight incubation, the ethanol was removed and the cells were washed and stained with 300 µM propidium iodine and 30 µg/ml RNase A in PBS at room temperature for 30 min. DNA content was analysed from 20 000 cells using the CyAn™ ADP Analyzer flow cytometer.

Caenorhabditis elegans methods

All nematodes strains were grown and maintained under standard conditions on NGM (nematode growth media) plates seeded with OP50 *Escherichia coli* incubated at 15 or 20°C (60). The *nekl-1p::gfp* transcriptional reporter construct was generated by fusion PCR (61). The intergenic *nekl-1* 5′UTR (promoter) sequence of 1583 bp was first amplified from *C. elegans* genomic DNA and then fused to an NLS::GFP fragment amplified from plasmid pPD95-67. Construct was microinjected at 50 ng/µl along with the co-injection marker *unc-122p::dsRed* (at 100 ng/µl) into N2 Bristol hermaphrodites (P0) to generate transgenic worms expressing *nekl-1p::gfp* as an extrachromosomal array. Multiple transgenic lines were observed and transgene expression compared. The DiI incorporation assay was conducted as previously described (62). For imaging, live worms were immobilized using levamisole 40 mM and mounted on 4% agarose pad. Imaging was performed using a Leica DM5000b epifluorescence compound microscope and images analysed with ImageJ (FIJI) software.

Supplementary Material

Supplementary material is available at *HMG* online.

Acknowledgements

We sincerely thank the participating families for their significant contribution to research and permission to use genetic samples and clinical information. We would like to thank Rhona Macleod Prof. Dian Donnai and Dr Emma Burkitt Wright (Manchester Centre for Genomic Medicine) for their valuable help with the families and clinical input. We would also like to thank Dr Sahar Mansour (SW Thames Regional Genetics Service, St George's Healthcare NHS Trust, London, UK) for her clinical input and helpful discussions of skeletal dysplasias.

Conflict of Interest statement: None declared.

Funding

This work was supported by a Medical Research Charities Group award co-funded by the Health Research Board (Ireland) and the Children's Fund for Health, Temple Street Children's University Hospital (Dublin, Ireland) (MRCG/2013/02 to S.A.L. and J. P. C.). The C. elegans studies were supported by a Science Foundation Ireland principal investigator award (SFI-11-1037) to O.E.B.

References

1. Warman, M.L., Cormier-Daire, V., Hall, C., Krakow, D., Lachman, R., LeMerrer, M., Mortier, G., Mundlos, S., Nishimura, G., Rimoin, D.L. *et al.* (2011) Nosology and classification of genetic skeletal disorders: 2010 revision. *Am. J. Med. Genet. A*, **155A**, 943–968.
2. Krakow, D., Lachman, R.S. and Rimoin, D.L. (2009) Guidelines for the prenatal diagnosis of fetal skeletal dysplasias. *Genet. Med.*, **11**, 127–133.
3. Donnelly, D.E., McConnell, V., Paterson, A. and Morrison, P.J. (2010) The prevalence of thanatophoric dysplasia and lethal osteogenesis imperfecta type II in Northern Ireland—a complete population study. *Ulster Med. J.*, **79**, 114–118.
4. Krakow, D., Alanay, Y., Rimoin, L.P., Lin, V., Wilcox, W.R., Lachman, R.S. and Rimoin, D.L. (2008) Evaluation of prenatal-onset osteochondrodysplasias by ultrasonography: a retrospective and prospective analysis. *Am. J. Med. Genet. A*, **146A**, 1917–1924.
5. Orioli, I.M., Castilla, E.E. and Barbosa-Neto, J.G. (1986) The birth prevalence rates for the skeletal dysplasias. *J. Med. Genet.*, **23**, 328–332.
6. Stoll, C., Dott, B., Roth, M.P. and Alembik, Y. (1989) Birth prevalence rates of skeletal dysplasias. *Clin. Genet.*, **35**, 88–92.
7. Shanske, A.L., Bernstein, L. and Herzog, R. (2007) Chondrodysplasia punctata and maternal autoimmune disease: a new case and review of the literature. *Pediatrics*, **120**, e436–e441.
8. Savarirayan, R. (1999) Common phenotype and etiology in warfarin embryopathy and X-linked chondrodysplasia punctata (CDPX). *Pediatr. Radiol.*, **29**, 322.
9. Baujat, G., Huber, C., El Hokayem, J., Caumes, R., Do Ngoc Thanh, C., David, A., Delezoide, A.-L., Dieux-Coeslier, A., Estournet, B., Francannet, C. *et al.* (2013) Asphyxiating thoracic dysplasia: clinical and molecular review of 39 families. *J. Med. Genet.*, **50**, 91–98.
10. Rossi, A. and Superti-Furga, A. (2001) Mutations in the diastrophic dysplasia sulfate transporter (DTDST) gene (SLC26A2): 22 novel mutations, mutation review, associated skeletal phenotypes, and diagnostic relevance. *Hum. Mutat.*, **17**, 159–171.
11. Chen, Y., Chen, C.-F., Riley, D.J. and Chen, P.-L. (2011) Nek1 kinase functions in DNA damage response and checkpoint control through a pathway independent of ATM and ATR. *Cell Cycle*, **10**, 655–663.
12. Meirelles, G.V., Perez, A.M., de Souza, E.E., Basei, F.L., Papa, P.F., Melo Hanchuk, T.D., Cardoso, V.B. and Kobarg, J. (2014) 'Stop Ne(c)king around': How interactomics contributes to functionally characterize Nek family kinases. *World J. Biol. Chem.*, **5**, 141–160.
13. Pelegrini, A.L., Moura, D.J., Brenner, B.L., Ledur, P.F., Maques, G.P., Henriques, J.A.P., Saffi, J. and Lenz, G. (2010) Nek1 silencing slows down DNA repair and blocks DNA damage-induced cell cycle arrest. *Mutagenesis*, **25**, 447–454.
14. Fry, A.M., O'Regan, L., Sabir, S.R. and Bayliss, R. (2012) Cell cycle regulation by the NEK family of protein kinases. *J. Cell Sci.*, **125**, 4423–4433.
15. Roig, J., Mikhailov, A., Belham, C. and Avruch, J. (2002) Nercc1, a mammalian NIMA-family kinase, binds the Ran GTPase and regulates mitotic progression. *Genes Dev.*, **16**, 1640–1658.
16. Kaneta, Y. and Ullrich, A. (2013) NEK9 depletion induces catastrophic mitosis by impairment of mitotic checkpoint control and spindle dynamics. *Biochem. Biophys. Res. Commun.*, **442**, 139–146.
17. Yang, S.-W., Gao, C., Chen, L., Song, Y.-L., Zhu, J.-L., Qi, S.-T., Jiang, Z.-Z., Wang, Z.-W., Lin, F., Huang, H. *et al.* (2012) Nek9 regulates spindle organization and cell cycle progression during mouse oocyte meiosis and its location in early embryo mitosis. *Cell Cycle*, **11**, 4366–4377.
18. Orphanides, G., Wu, W.H., Lane, W.S., Hampsey, M. and Reinberg, D. (1999) The chromatin-specific transcription elongation factor FACT comprises human SPT16 and SSRP1 proteins. *Nature*, **400**, 284–288.
19. Tan, B.C.-M. and Lee, S.-C. (2004) Nek9, a novel FACT-associated protein, modulates interphase progression. *J. Biol. Chem.*, **279**, 9321–9330.
20. Huber, C., Wu, S., Kim, A.S., Sigaudy, S., Sarukhanov, A., Serre, V., Baujat, G., Le Quan Sang, K.-H., Rimoin, D.L., Cohn, D.H. *et al.* (2013) WDR34 mutations that cause short-rib polydactyly syndrome type III/severe asphyxiating thoracic dysplasia reveal a role for the NF-κB pathway in cilia. *Am. J. Hum. Genet.*, **93**, 926–931.
21. Taylor, S.P., Dantas, T.J., Duran, I., Wu, S., Lachman, R.S., Nelson, S.F., Cohn, D.H., Vallee, R.B. and Krakow, D. (2015) Mutations in DYNC2LI1 disrupt cilia function and cause short rib polydactyly syndrome. *Nat. Commun.*, **6**, 7092.
22. Thiel, C., Kessler, K., Giessl, A., Dimmler, A., Shalev, S.A., von der Haar, S., Zenker, M., Zahnleiter, D., Stöss, H., Beinder, E. *et al.* (2011) NEK1 mutations cause short-rib polydactyly syndrome type Majewski. *Am. J. Hum. Genet.*, **88**, 106–114.
23. Inglis, P.N., Ou, G., Leroux, M.R. and Scholey, J.M. (2007) The sensory cilia of *Caenorhabditis elegans*. *WormBook*. The C. elegans Research Community, WormBook, doi/10.1895/wormbook.1.126.2. http://www.wormbook.org.
24. Reiter, J.F., Blacque, O.E. and Leroux, M.R. (2012) The base of the cilium: roles for transition fibres and the transition zone in ciliary formation, maintenance and compartmentalization. *EMBO Rep.*, **13**, 608–618.
25. Blacque, O.E. and Sanders, A.A.W.M. (2014) Compartments within a compartment: what *C. elegans* can tell us about ciliary subdomain composition, biogenesis, function, and disease. *Organogenesis*, **10**, 126–137.
26. Lupas, A., Van Dyke, M. and Stock, J. (1991) Predicting coiled coils from protein sequences. *Science*, **252**, 1162–1164.
27. Starich, T.A., Herman, R.K., Kari, C.K., Yeh, W.H., Schackwitz, W.S., Schuyler, M.W., Collet, J., Thomas, J.H. and Riddle, D.L. (1995) Mutations affecting the chemosensory neurons of *Caenorhabditis elegans*. *Genetics*, **139**, 171–188.
28. Honkala, H., Lahtela, J., Fox, H., Gentile, M., Pakkasjärvi, N., Salonen, R., Wartiovaara, K., Jauhiainen, M. and Kestilä, M. (2009) Unraveling the disease pathogenesis behind lethal hydrolethalus syndrome revealed multiple changes in molecular and cellular level. *Pathogenetics*, **2**, 2.
29. Patil, M., Pabla, N., Ding, H.-F. and Dong, Z. (2013) Nek1 interacts with Ku80 to assist chromatin loading of replication factors and S-phase progression. *Cell Cycle*, **12**, 2608–2616.
30. Vaux, D.L. and Korsmeyer, S.J. (1999) Cell death in development. *Cell*, **96**, 245–254.
31. El-Hashash, A.H.K., Al Alam, D., Turcatel, G., Bellusci, S. and Warburton, D. (2011) Eyes absent 1 (Eya1) is a critical

coordinator of epithelial, mesenchymal and vascular morphogenesis in the mammalian lung. *Dev. Biol.*, **350**, 112–126.
32. Baguma-Nibasheka, M. and Kablar, B. (2008) Pulmonary hypoplasia in the connective tissue growth factor (CTGF) null mouse. *Dev. Dyn.*, **237**, 485–493.
33. van Loenhout, R.B., Tseu, I., Fox, E.K., Huang, Z., Tibboel, D., Post, M. and Keijzer, R. (2012) The pulmonary mesenchymal tissue layer is defective in an in vitro recombinant model of nitrofen-induced lung hypoplasia. *Am. J. Pathol.*, **180**, 48–60.
34. O'regan, L., Blot, J. and Fry, A.M. (2007) Mitotic regulation by NIMA-related kinases. *Cell Div.*, **2**, 25.
35. Moniz, L., Dutt, P., Haider, N. and Stambolic, V. (2011) Nek family of kinases in cell cycle, checkpoint control and cancer. *Cell Div.*, **6**, 18.
36. Nishiguchi, K.M., Tearle, R.G., Liu, Y.P., Oh, E.C., Miyake, N., Benaglio, P., Harper, S., Koskiniemi-Kuendig, H., Venturini, G., Sharon, D. *et al.* (2013) Whole genome sequencing in patients with retinitis pigmentosa reveals pathogenic DNA structural changes and NEK2 as a new disease gene. *Proc. Natl. Acad. Sci. U. S. A.*, **110**, 16139–16144.
37. Fakhro, K.A., Choi, M., Ware, S.M., Belmont, J.W., Towbin, J.A., Lifton, R.P., Khokha, M.K. and Brueckner, M. (2011) Rare copy number variations in congenital heart disease patients identify unique genes in left-right patterning. *Proc. Natl. Acad. Sci. U. S. A.*, **108**, 2915–2920.
38. Otto, E.A., Trapp, M.L., Schultheiss, U.T., Helou, J., Quarmby, L.M. and Hildebrandt, F. (2008) NEK8 mutations affect ciliary and centrosomal localization and may cause nephronophthisis. *J. Am. Soc. Nephrol.*, **19**, 587–592.
39. Frank, V., Habbig, S., Bartram, M.P., Eisenberger, T., Veenstra-Knol, H.E., Decker, C., Boorsma, R.A.C., Göbel, H., Nürnberg, G., Griessmann, A. *et al.* (2013) Mutations in NEK8 link multiple organ dysplasia with altered Hippo signalling and increased c-MYC expression. *Hum. Mol. Genet.*, **22**, 2177–2185.
40. Salem, H., Rachmin, I., Yissachar, N., Cohen, S., Amiel, A., Haffner, R., Lavi, L. and Motro, B. (2010) Nek7 kinase targeting leads to early mortality, cytokinesis disturbance and polyploidy. *Oncogene*, **29**, 4046–4057.
41. Mahjoub, M.R., Trapp, M.L. and Quarmby, L.M. (2005) NIMA-related kinases defective in murine models of polycystic kidney diseases localize to primary cilia and centrosomes. *J. Am. Soc. Nephrol.*, **16**, 3485–3489.
42. Vogler, C., Homan, S., Pung, A., Thorpe, C., Barker, J., Birkenmeier, E.H. and Upadhya, P. (1999) Clinical and pathologic findings in two new allelic murine models of polycystic kidney disease. *J. Am. Soc. Nephrol.*, **10**, 2534–2539.
43. Zalli, D., Bayliss, R. and Fry, A.M. (2012) The Nek8 protein kinase, mutated in the human cystic kidney disease nephronophthisis, is both activated and degraded during ciliogenesis. *Hum. Mol. Genet.*, **21**, 1155–1171.
44. Bowers, A.J. and Boylan, J.F. (2004) Nek8, a NIMA family kinase member, is overexpressed in primary human breast tumors. *Gene*, **328**, 135–142.
45. Hadjebi, O., Casas-Terradellas, E., Garcia-Gonzalo, F.R. and Rosa, J.L. (2008) The RCC1 superfamily: from genes, to function, to disease. *Biochim. Biophys. Acta*, **1783**, 1467–1479.
46. Bertran, M.T., Sdelci, S., Regué, L., Avruch, J., Caelles, C. and Roig, J. (2011) Nek9 is a Plk1-activated kinase that controls early centrosome separation through Nek6/7 and Eg5. *EMBO J.*, **30**, 2634–2647.
47. Vigneault, F., Lachance, D., Cloutier, M., Pelletier, G., Levasseur, C. and Séguin, A. (2007) Members of the plant NIMA-related kinases are involved in organ development and vascularization in poplar, Arabidopsis and rice. *Plant J.*, **51**, 575–588.
48. Hunter, J.M., Kiefer, J., Balak, C.D., Jooma, S., Ahearn, M.E., Hall, J.G. and Baumbach-Reardon, L. (2015) Review of X-linked syndromes with arthrogryposis or early contractures-aid to diagnosis and pathway identification. *Am. J. Med. Genet. A*, **167A**, 931–973.
49. Coene, K.L.M., Roepman, R., Doherty, D., Afroze, B., Kroes, H.Y., Letteboer, S.J.F., Ngu, L.H., Budny, B., van Wijk, E., Gorden, N.T. *et al.* (2009) OFD1 is mutated in X-linked Joubert syndrome and interacts with LCA5-encoded lebercilin. *Am. J. Hum. Genet.*, **85**, 465–481.
50. Badano, J.L., Mitsuma, N., Beales, P.L. and Katsanis, N. (2006) The ciliopathies: an emerging class of human genetic disorders. *Annu. Rev. Genomics Hum. Genet.*, **7**, 125–148.
51. McMillin, M.J., Beck, A.E., Chong, J.X., Shively, K.M., Buckingham, K.J., Gildersleeve, H.I.S., Aracena, M.I., Aylsworth, A.S., Bitoun, P., Carey, J.C. *et al.* (2014) Mutations in PIEZO2 cause Gordon syndrome, Marden-Walker syndrome, and distal arthrogryposis type 5. *Am. J. Hum. Genet.*, **94**, 734–744.
52. Lehman, J.M., Michaud, E.J., Schoeb, T.R., Aydin-Son, Y., Miller, M. and Yoder, B.K. (2008) The Oak Ridge polycystic kidney mouse: modeling ciliopathies of mice and men. *Dev. Dyn.*, **237**, 1960–1971.
53. Juric-Sekhar, G., Adkins, J., Doherty, D. and Hevner, R.F. (2012) Joubert syndrome: brain and spinal cord malformations in genotyped cases and implications for neurodevelopmental functions of primary cilia. *Acta Neuropathol.*, **123**, 695–709.
54. Marshall, W.F. (2008) The cell biological basis of ciliary disease. *J. Cell Biol.*, **180**, 17–21.
55. Purcell, S., Neale, B., Todd-Brown, K., Thomas, L., Ferreira, M. A.R., Bender, D., Maller, J., Sklar, P., de Bakker, P.I.W., Daly, M.J. *et al.* (2007) PLINK: a tool set for whole-genome association and population-based linkage analyses. *Am. J. Hum. Genet.*, **81**, 559–575.
56. Li, H. and Durbin, R. (2009) Fast and accurate short read alignment with Burrows-Wheeler transform. *Bioinformatics*, **25**, 1754–1760.
57. McKenna, A., Hanna, M., Banks, E., Sivachenko, A., Cibulskis, K., Kernytsky, A., Garimella, K., Altshuler, D., Gabriel, S., Daly, M. *et al.* (2010) The Genome Analysis Toolkit: a MapReduce framework for analyzing next-generation DNA sequencing data. *Genome Res.*, **20**, 1297–1303.
58. Li, H., Handsaker, B., Wysoker, A., Fennell, T., Ruan, J., Homer, N., Marth, G., Abecasis, G. and Durbin, R. (2009) The sequence alignment/map format and SAMtools. *Bioinformatics*, **25**, 2078–2079.
59. Wang, K., Li, M. and Hakonarson, H. (2010) ANNOVAR: functional annotation of genetic variants from high-throughput sequencing data. *Nucleic Acids Res.*, **38**, e164.
60. Brenner, S. (1974) The genetics of *Caenorhabditis elegans*. *Genetics*, **77**, 71–94.
61. Hobert, O. (2002) PCR fusion-based approach to create reporter gene constructs for expression analysis in transgenic *C. elegans*. *Biotechniques*, **32**, 728–730.
62. Sanders, A.A.W.M., Kennedy, J. and Blacque, O.E. (2015) Image analysis of *Caenorhabditis elegans* ciliary transition zone structure, ultrastructure, molecular composition, and function. *Methods Cell Biol.*, **127**, 323–347.